Proc. Int. Symp. for Ultra-High Energy Cosmic Rays (UHECR2014)
JPS Conf. Proc. **9**, 010009 (2016)
http://doi.org/10.7566/JPSCP.9.010009

.

The Primary CR Spectrum by the Data of the Tunka-133 Array

S.F. Berezhnev[1], N.M. Budnev[2], A. Chiavassa[4] , O.A. Chvalaev[2], O.A. Gress[2], T.I. Gress[2], A.N. Dyachok[2], S.N. Epimakhov[6], N.I. Karpov[1], N.N. Kalmykov[1], E.N. Konstantinov[2], A.V. Korobchenko[2], E.E. Korosteleva[1], V.A. Kozhin[1], L.A. Kuzmichev[1,2], B.K. Lubsandorzhiev[3], N.B. Lubsandorzhiev[1], R.R. Mirgazov[2], R.D. Monkhoev[2], E.A. Osipova[1], A.L. Pakhorukov[2], M.I. Panasyuk[1], L.V. Pankov[2], E.G. Popova[1], V.V. Prosin[1], V.S. Ptuskin[7], Yu.A. Semeney[2], A.A. Silaev[1], A.A. Silaev(junior)[1], A.V. Skurikhin[1], C. Spiering[5], L.G. Sveshnikova[1], A.V. Zagorodnikov[2]

[1]*Skobeltsyn Institute of Nuclear Physics MSU, Moscow, Russian Federation*
[2]*Irkutsk State University, Irkutsk, Russian Federation*
[3]*]Institute for Nuclear Research of the Russian Academy of Sciences, Russian Federation*
[4]*Dipartimento di Fisica Generale dell'Universita' and INFN,Torino, Italy*
[5]*DESY, Zeuthen, Germany*
[6]*Hamburg University, Hamburg, Germany*
[7]*IZMIRAN, Troitsk, Russia*

E-mail: kuz@dec1.sinp.msu.ru

The Cherenkov-light EAS array Tunka-133, with $\sim 3\,\mathrm{km}^2$ geometric area, is taking data since 2009. The array permits a detailed study of energy spectrum and mass composition of cosmic rays in the energy range from $5 \cdot 10^{15}$ to 10^{18} eV. We describe the array construction, the DAQ and the array calibration and discuss the method of energy reconstruction and absolute calibration. We present the all-particle energy spectrum based on 5 seasons of array operation. In the last part of the paper, we discuss possible interpretations of the obtained results and sketch plans for upgrading the array

KEYWORDS: UHECR-2014, Tunka-133, Cherenkov radiation, energy spectrum . . .

1. Introduction

The study of primary energy spectrum and mass composition in the energy range of 10^{15} - 10^{18} eV is of crucial importance for understanding origin and propagation of cosmic rays (CR) in the Galaxy.

One of the most informative methods of cosmic ray studies is the registration of Cherenkov light from Extensive Air Showers (EAS). The uncertainty of primary energy reconstruction is strongly reduced by using the Earth's atmosphere as a huge calorimeter. This is achieved by recording the optical radiation from EAS during clear, moonless nights. The atmosphere, in the absence of clouds and aerosols, is remarkably transparent for visible light. Molecular scattering leads to losses of only 15% of light, the losses from aerosol scattering are of a similar size.

To study CR with the help of Cherenkov light, the Tunka-133 array ([1], [2]) with nearly $3\,\mathrm{km}^2$ geometrical area has been deployed in the Tunka Valley, Siberia. The array began operation in October 2009. Results presented in this paper are based on data registered during 5 winter seasons. The total time of data taking is 1540 hrs. The number of recorded events is about 10^7.

2. The Tunka-133 Array

The Tunka-133 array is located in the Tunka Valley (50 km from Lake Baikal), at an altitude of 670 m a.s.l. Tunka-133 consists of 175 optical detectors on the basis of PMT EMI 9350 with a hemispherical photocathode of 20 cm diameter.

The detectors are grouped into 25 clusters, each with 7 detectors – six hexagonally arranged detectors and one in the center. The distance between the detectors in the cluster is 85 m (see Fig.1). 19 clusters are installed in an inner circle of 500 m radius ("inside" clusters), 6 clusters were placed at the distance of 700 – 1000 m from the center ("outside" clusters).

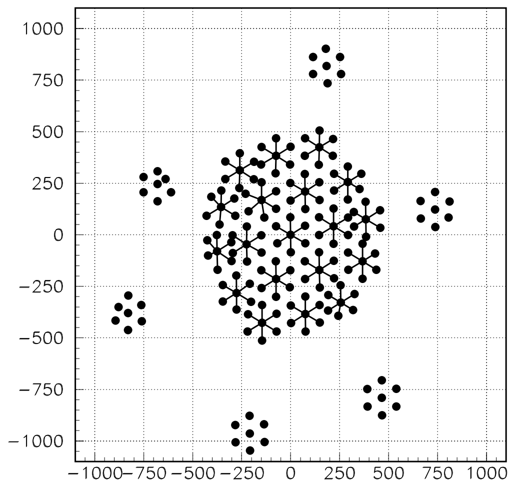

Fig. 1. Layout of the Tunka-133 array.

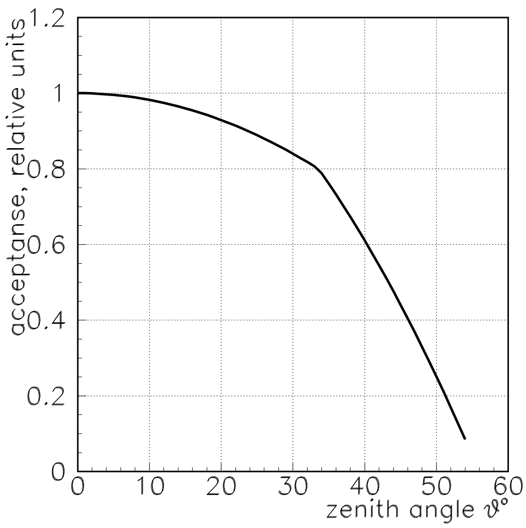

Fig. 2. Acceptance of the optical detector.

An optical detector consists of a 50 cm diameter metallic cylinder, containing a PMT. The container window is directed to zenith and covered with plexiglass heated against hoar-frost and dew. The detector is equipped with a remotely controlled lid protecting the PMT from sunlight and precipitation.

The PMT output pulses are sent via 95 m coaxial cable RG58 to the center of a cluster and digitized. The dynamic range of the amplitude measurement is about $3 \cdot 10^4$. This is achieved by means of two channels for each detector extracting the signals from the anode and an intermediate dynode of the PMT with different additional amplification factors.

The cluster electronics includes the cluster controller, 4 four-channel FADC boards, an adapter unit for connection with optical detectors and a special temperature controller. The 12 bit and 200 MHz sampling FADC board is based on AD9430 fast ADCs and FPGA XILINX Spartan XC3S300 microchips. The cluster controller consists of an optical transceiver, a synchronization module, a local time clock and a trigger module. The optical transceiver operating at 1000 MHz is responsible for data transmission and formation of 100 MHz synchronization signals for the cluster clocks. The cluster trigger (the local trigger) is formed by the coincidence of at least three pulses from the optical detectors exceeding the threshold within a time window of 0.5 μs. The time mark of the local trigger is fixed by the cluster clock. The accuracy of the time synchronization between different clusters is about 10 ns. Each cluster electronics is connected with the DAQ center by a multi-wire cable containing four copper wires and four optical fibers.

The central DAQ station consists of 4 DAQ boards synchronized by a single 100 MHz generator. The boards are connected with the master PC by 100 MHz Ethernet lines.

The detector efficiency vs. the zenith angle is shown in Fig.2. This curve reflects the influence of the window edge as well as the atmosphere absorption due to Rayleigh and aerosol scattering of the Cherenkov light. The measured light flux was divided by this function to get the correct value of light flux proportional to the primary energy. To check the simulated efficiency we analyse the zenith angle distribution of the recorded EAS with energy more than a fixed value. The resulting zenith angle distribution of EAS with energies larger than 15 PeV is presented in Fig.3. The distribution is uniform till an angle of 50°.

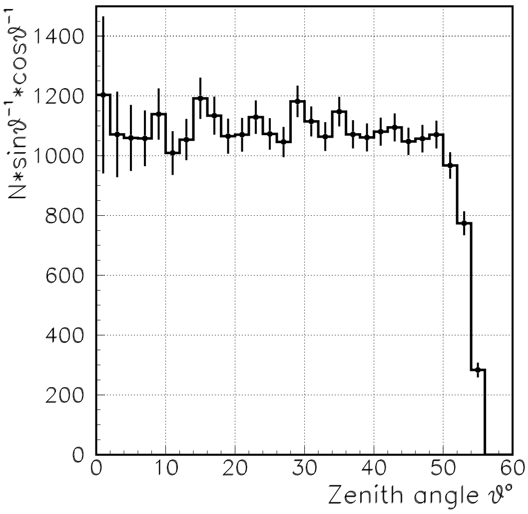

Fig. 3. Zenith angle distribution.

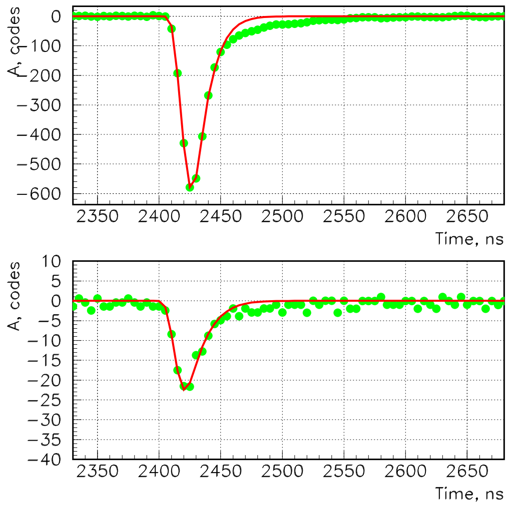

Fig. 4. Example of a pulse from one Tunka-133 detector, recorded by high and low gain channels

The amplitude calibration of the detectors was carried out in two steps similar to that used at the previous experiment Tunka-25. The details are described in [3].

3. Data processing and reconstruction of EAS parameters

3.1 Data processing

The primary data record for each Cherenkov light detector contains 1024 amplitude values with a step of 5 ns (Fig.4). Thus each pulse waveform is recorded together with the preceding noise as a trace of 5 μs. To derive three main parameters of the pulse: front delay at a level 0.25 of the maximum amplitude t_i, maximum amplitude A_i pulse area Q_i, each pulse is fitted with a special self-designed smoothing curve [4]. A fourth pulse parameter is the effective width τ_{eff} which equals to $Q_i/(1.24 \cdot A_i)$. The accuracy of this parameter is better than that of the pulse width (FWHM) used earlier. The additional coefficient (1.24) "normalizes" τ_{eff} to FWHM.

3.2 Timing calibration

The timing calibration of the detectors is made with the recorded air shower data. The calibration inside of a single cluster consists of a multiple reconstruction of zenith θ and azimuth ϕ angles for all recorded showers with analysis of the residual differences between measured data and model description. At this step we use a plane front model. The model with a curved shower front described below demand the knowledge of the EAS core position. The difference between the modelled plane and the real curve front leads to an increase of the residual ΔT standard deviation but doesn't distort very much the mean values of ΔT because of the almost uniform core distribution inside the cluster area.

The residual ΔT is treated as an additional apparatus shift, and it is added to the calibration shift. Then the procedure of the arrival direction reconstruction is repeated once again times all the detector shifts becomes less than $\Delta T = 1$ ns.

The obtained calibration corrections are used for preliminary reconstruction of the EAS core position with a plane model of the shower front using a single cluster selected with the largest amplitudes of pulses.

At the second step of the timing calibration we select large showers with more than 8 hit clusters and reconstruct the shower front assuming a curved shape derived from CORSIKA simulations and described in the next section.

The space basement of the pulse delay analysis is more than 500 m for such events. So the apparatus error of cluster synchronization (about 10 ns) can lead to a maximum error in the arrival direction of only 0.4°.

During this step we correct the calibration coefficients a second time so that the EAS axis direction measured by each single cluster coincides with the axis direction from the multi-cluster method with an accuracy better than 0.5°. The calibration constants are the relative delay of each cluster central detector and the delays of peripheral detectors relatively the central one. The last correction is made synchronously for all the 6 detectors to rotate the plane reconstructed by the cluster parallel to the surface of the EAS front at the point of the cluster center.

3.3 Arrival direction

The shower arrival direction, characterized by zenith θ and azimuth ϕ angles, is reconstructed by fitting the measured delays with a curved shower front: $\Delta T = T_i - T_f = R \cdot (R + 500)/(c \cdot F)$, where T_f is the estimated delay for a plane front, R the perpendicular distance from the shower axis in meters, c the speed of light and F a variable parameter. This approximate formula is derived from the analysis of simulated showers by CORSIKA. The formula, on the one hand, has a non-zero value of the derivative at $R = 0$ (conical shape, typical for Cherenkov radiation at short distances from the axis) and on the other hand, has only one shape parameter which is essential for processing of relatively small showers. To obtain R one needs to know the EAS core position.

3.4 Core position

The reconstruction of the EAS core position is performed by fitting measured amplitudes A_i with an amplitude distance function (ADF):

$$A(R) = A(200) \cdot f(R) \tag{1}$$

The function $f(R)$ is a fit to four different parametrizations according to the distance R (in meters) to the shower core ([5]). Four variables in this parametrization (R_0, R_{kn}, a and b_2), describing the ADF shape in the different ranges of core distance are related to a single parameter of the ADF shape – the steepness b_A:

$$
\begin{aligned}
&d = b_A - 5, \lg d = \log\ d,\\
&R_0 = 275/d,\\
&R_{\mathrm{kn}} = 145 - 115 \cdot \lg d,\\
&a = 0.89 - 0.29 \cdot \lg d,\\
&b_2 = \begin{cases} 2.4 + 2 \cdot (\lg d - 0.15), & b_A \geq 6.41 \\ 2.4, & b_A < 6.41 \end{cases}
\end{aligned}
\tag{2}
$$

The ADF steepness parameter b_A is treated as independent variable during the minimisation procedure. But if two other independent variables the core coordinates define the core position far from the dense parts of the array b_A is treated as a fixed parameter. Its value is derived from the value of X_{max}, obtained from the mean width τ_{eff} of Cherenkov light pulses at a distance of 400 m to the core. The connection τ_{eff} vs. X_{max} and b_A vs. X_{max} has been obtained and was discussed in [5].

3.5 Energy reconstruction

As a measure of energy we use the Cherenkov light flux density at a core distance of 200 m - $Q(200)$. Reconstruction of $Q(200)$ is made by fitting the measured values of Q_i with the lateral distribution function (LDF) [5]. The connection between the EAS energy E_0 and $Q(200)$ can be expressed by the following formula:

$$E_0 = C \cdot Q(200)^g \tag{3}$$

For an energy range of $10^{16} - 10^{18}$ eV, a zenith angle range of $0° - 45°$ and a complex composition, consisting of equal contribution of protons and iron nuclei, CORSIKA simulations provide an index g=0.94.

To reconstruct the EAS energy from the Cherenkov light flux one needs to know the absolute sensitivities of the Cherenkov detectors and the atmosphere transparency. To avoid these problems, the method of normalization of the integral energy spectrum to a reference spectrum is used. The reference energy spectrum was measured by the QUEST experiment [6], [7]. The integral energy spectrum obtained for each night of the Tunka-133 operation is normalised to that reference spectrum.

An example of core reconstruction is presented in Fig.5. The ADF and LDF functions for this event are presented in Fig.6.

4. Energy Spectrum

4.1 Experimental data

The Cherenkov light array Tunka-133 operates in clear moonless nights between October and early April. During the rest of the year, the nights are too short and the weather conditions are mostly unsatisfactory. Tunka-133 took data during 5 winter seasons 2009-2010 to 2013-2014. Here we present the data of these 5 seasons. The total time of data acquisition is 1540 hrs. The mean trigger rate was about 2 Hz. The number of recorded events is about 10^7. Such an amount of recorded data provided the possibility of calibration of the apparatus using the data themselves.

4.2 Energy spectrum reconstruction

To reconstruct the Tunka-133 spectrum we selected events with zenith angles $\theta \leq 45°$ and the core position inside a circle of radius $R_c \leq 450$ m for energy $E_0 < 5 \cdot 10^{16}$ eV and a circle of radius $R_c < 800$ m for showers with energy $E_0 \geq 5 \cdot 10^{16}$ eV. Comparison of the spectra for these two effective areas showed that starting from the above mentioned energy

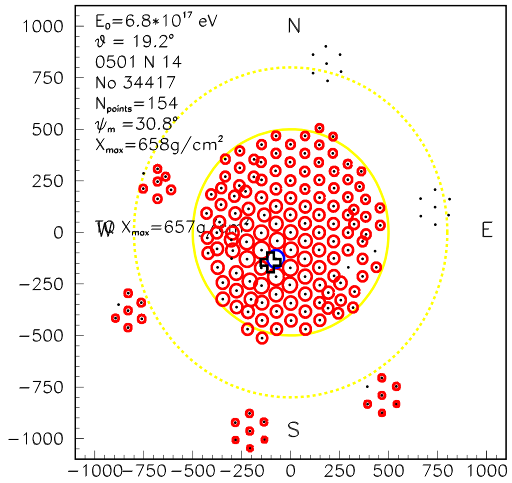

Fig. 5. An example of experimental EAS core reconstruction. The radius of each station circle is proportional to the $logQ_i$.

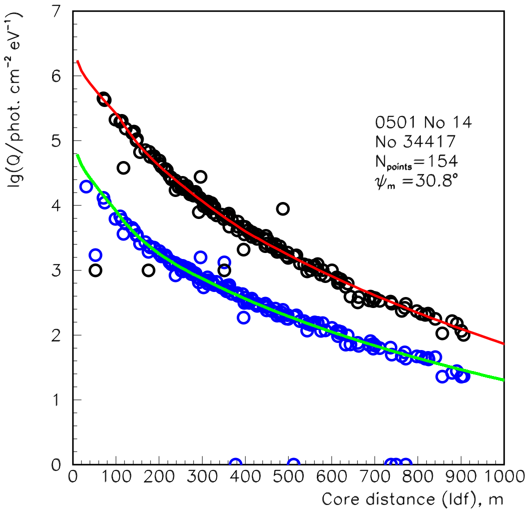

Fig. 6. An example of experimental EAS pulse amplitudes fitting with ADF and resulting LDF.

spectra within the error bars are the same, but the event statistics in the second case is three times larger which is essential for energies $E_0 \geq 10^{17}$ eV.

The efficiency of shower selection inside the circle with $R_c \leq 450$ m reaches 100% for energies $E_0 \geq 6 \cdot 10^{15}$ eV. The total number of events above this energy is 270000. About 3000 events, selected in the circle with $R_c < 800$ m have $E_0 \geq 10^{17}$ eV.

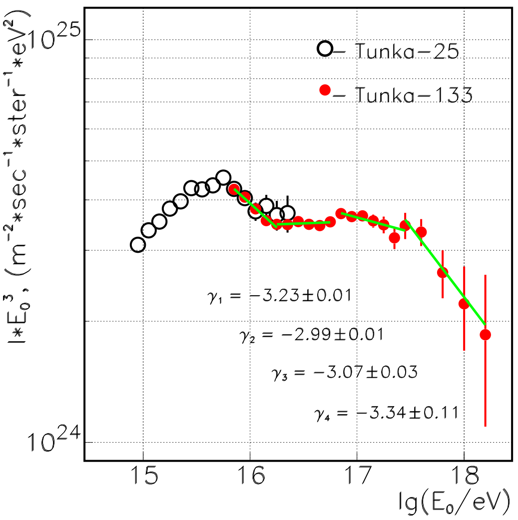

Fig. 7. Differential primary cosmic ray energy spectrum.

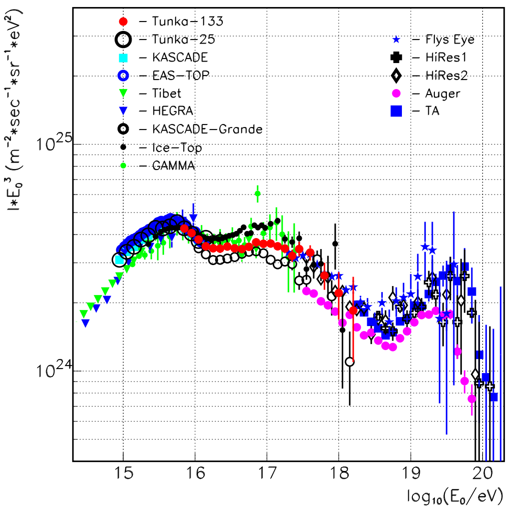

Fig. 8. Comparison of energy spectra obtained at Tunka with some other experiments.

The resulting differential energy spectrum is shown in Fig.7 along with the previous spectrum of Tunka-25 [3]. The spectrum of Tunka-133 shows a number of features - deviations from the power law. One can interpret the picture as a much more complicated behavior than a power law (or multiply broken power law). The power-law description can be used only for small parts of the spectrum – not more than half an order of magnitude. At the energy of about $2 \cdot 10^{16}$ eV the power law index changes from $\gamma = 3.23 \pm 0.01$ to $\gamma = 2.99 \pm 0.01$. This feature was first observed in the KASCADE-Grande experiment [8]. Points of the spectrum are consistent with such an index till the energy $E_0 = 5 \cdot 10^{16}$ eV. Above this energy one can notice a single point deflecting from the power-law description by about 2 standard deviations. The energy of this point ($6.3 \cdot 10^{16}$ eV) coincides with that for a "peak", observed in the GAMMA experiment [9]. Between this point and $E_0 = 3 \cdot 10^{17}$ the index is $\gamma = 3.07 \pm 0.03$ The spectrum becomes much steeper with $\gamma = 3.34 \pm 0.11$ above the last point (the second "knee").

4.3 Comparison of Tunka-133 energy spectrum with results of other experiments

In Fig.8 the spectrum is compared with a number of other experimental data. The spectra of all the experiments shown in Fig.8: KASCADE [10], EAS-TOP [11], Tibet [12], HEGRA [13] - are practically indistinguishable at the energy of the first (classical) knee.

There is an agreement between the result of Tunka-133 and the spectra of GAMMA [9], KASCADE-Grande [8] and Ice-TOP [14] in the intermediate energy range $10^{16} - 10^{17}$ eV. Noticeably, in Fig.8, the difference among the spectra at E_0 about 10^{17} eV can be eliminated by an energy correction of only 3%. Such an energy shift is much smaller than the absolute accuracy of these experiments.

For the high-energy edge, the Tunka-133 spectrum is in agreement with Fly's Eye [15], HiRes [16] and Telescope Array (TA) [17] data, and also (to less extend) with Auger [18].

The fine structure of the spectrum in the range of $10^{15} - 10^{17}$ eV does not contradict the so called rigidity dependent model of the knee origin [19]: any single galactic source provided the knee [20], accelerate particles up to limited maximal energy depending on the charge of nucleus Z, $E_{max}(Z) = Z \cdot E_{max}(Z = 1)$. In this interpretation the position of the first (classical) knee $3 \cdot 10^{15}$ eV corresponds to the proton cut-off, and the energy $8 \cdot 10^{16}$ eV indicates the cut-off of iron nuclei ($Z = 26$). The existence of more energetic particles can demand the discussion of the new galactic sources of unknown nature or (less probable) extragalactic sources.

5. Futher Experiments in Tunka Valley

5.1 Tunka-Grande: a net of scintillation stations

The deployment of 19 scintillation stations will be completed in 2015. This array (called Tunka-Grande) consists of scintillation counters from the former KASCADE-Grande array. The stations are located near the centers of Tunka-133 clusters. Thus the effective area of the array is about 1 km^2. In each station 12 detectors are located on the ground surface and 8 detectors - underground for registration of muons. All the surface parts and 8 underground parts of the stations have been already installed.

Tunka-Grande DAQ, synchronization and control systems are similar to that used in Tunka-133. Common operation of Tunka-133 and Tunka-Grande will allow a more precise study of mass composition at the upper edge of the Galactic energy spectrum.

5.2 Tunka-REX

The Tunka-Rex (Tunka Radio extension) array [21] consists of 44 antennas deployed at the area of about 3 km^2. Among them 38 antennas are installed in the central dense part of Tunka-133 array of 500 m radius. Antennas can operate under both Tunka-133 or Tunka-Grande triggers. The first common operation of Tunka-REX and Tunka-133 has shown that radio measurement of the primary energy provides almost the same accuracy as Cherenkov light measurement if the main EAS parameters (arrival direction and core position) are reconstructed by the data of Tunka-133 [22]. Common operation of Tunka-REX and Tunka-Grande will provide much more statistics in the energy range $10^{17} - 5 \cdot 10^{18}$ eV due to the total day and night duty cycle.

6. Conclusion

1. The primary CR energy spectrum in the range of $6 \cdot 10^{15} - 10^{18}$ eV has a number of features: the spectrum becomes harder (the index changes from $\gamma = 3.23 \pm 0.01$ to $\gamma = 2.99 \pm 0.01$) at $E_0 = 2 \cdot 10^{16}$ eV, then steeper with $\gamma = 3.07 \pm 0.03$ at $E_0 = 6.3 \cdot 10^{16}$ eV, and finally even more steeper ($\gamma = 3.34 \pm 0.11$) at $E_0 = 3 \cdot 10^{17}$ eV.
2. In the energy range of $10^{16} - 10^{17}$ eV, the Tunka-133 spectrum is consistent with the spectra of KASCADE-Grande [8] and IceTop [14].
3. Beyond the energy 10^{17} eV, the Tunka-133 spectrum is consistent with fluorescent light experiments Fly's Eye [15] and HIRES [16] and with the hybrid experiment TA [17].

7. Acknowledgment

This work was supported by the Ministry of Education and Science of the Russian Federation (State Contract 14.V25.31.0010, project 1366, zadanie N 3.889.2014/K), the Russian Foundation for Basic Research (grants 13-02-12095, 13-02-00214, 15-02-05769, 15-02-10005).

References

[1] Berezhnev F. et al. (Tunka Collaboration), Nucl. Instr. and Methods in Physics Research A **692**, 98 (2012)
[2] Antokhonov B. et al. (Tunka Collaboration), Nuclear Physics B (Proc. Suppl.) **212-213**, 247 (2011)
[3] Budnev N., et al., Astropart. Phys. **50**, 18-25 (2013)
[4] Korosteleva E.E. et al., Proc. 31st ICRC Lodz **ID=492**, (2009)
[5] Prosin V.V., et al., Nucl. Instr. and Methods in Physics Research A **756**, 94 (2014)
[6] E.Korosteleva et al., Int.J.Mod Phys. A20 (2005) 6837-6839, arXiv: astro-ph/0411216
[7] E.E. Korosteleva et al., Nuclear Physics B (Proc. Supp.), 2007 **165**: 74-80
[8] Apel W.D., et al. (KASCADE-Gr. Collaboration), Astropart. Phys. **36**, 183 (2012)
[9] Garyaka A.P., et al., Journal of Physics G: Nuclear and Particle Physics **ID=35**, 115201 (2008)
[10] Antony T., et al., Nucl. Instr. and Methods in Physics Research A **513**, 490 (2003)
[11] Aglietta M., et al., EAS-TOP Collaboration, Astropart. Phys. **10**, 1 (1999)
[12] Amenomori M., et al., (Tibet Col.), Astrophys. J. **678**, 1165 (2008)
[13] Arqueros F., et al., The HEGRA Collaboration, Astron. Astrophys. **359**, 682 (2000)
[14] Aartsen M.G., et al., Phys. Rev. Lett. D **88**, 042004 (2013)
[15] Abu-Zayyad T., et al., Phys. Rev. Lett. **84**, 4276 (2000)
[16] Sokolsky P. for the HiRes Collaboration, Nuclear Physics B (Proc. Suppl.) **212-213**, 74 (2011)
[17] Abu-Zayyad T., et al., Astropart. Phys. **48**, 16 (2013)
[18] Schulz A. for the Pierre Auger Collaboration, Proc. 33rd ICRC Rio De Janeiro **ID=769**, (2013)
[19] Sveshnikova L., et al., Nuclear Physics B (Proc. Suppl.) **218-224**, 256 (2014)
[20] Erlykin A., Wolfendale A., Martirosov R., CERN-Courier **21**, 201 (2011)
[21] Kostunin D. for the Tunka-REX collaboration, Nucl. Instr. and Methods in Physics Research A **742**, 89 (2014)
[22] Schröder F. for the Tunka-REX collaboration, This Proceedings.